EFFECT OF SUB-MICRON GLASS FIBER ADDITION ON CAI STRENGTH OF UD-CFRP

RYOTARO MURAYAMA[1], KIYOTAKA OBUNAI[2] & KAZUYA OKUBO[2]
[1]Graduate School of Doshisha University, Japan.
[2]Department of Mechanical Engineering, Doshisha University, Japan.

ABSTRACT

The purpose of this study is to investigate the effect of the addition of sub-micron glass fiber (sGF) into the matrix of carbon fiber reinforced plastics (CFRP) on the impact energy absorption and Compressive after impact (CAI) strength of it. The unidirectional (UD)-CFRP was fabricated with UD-carbon fiber fabric and thermoset epoxy resin modified by adding 0.3wt% of sGF. For comparison, UD-CFRP made with the neat epoxy resin was also prepared. The impact energy absorption under out-of-plane impact was measured by using falling-type impact testing equipment. In this study, the applied impact energy was 3, 5, 7, 10, and 20 J by changing the mass of the drop weight. After the tests, a compressive load was also applied to the specimen to investigate the CAI strength of UD-CFRP. Test results showed that when the applied impact energy was relatively low (3 and 5 J), the energy absorption of the modified UD-CFRP was slightly improved, compared to that of the neat UD-CFRP. The projection areas of internal damages of UD-CFRP after the drop weight test were also decreased by the sGF addition. However, when the applied impact energy exceeds 7 J, there were no differences in the energy absorption of UD-CFRP even if the sGF was added to the matrix. The scanning electron microscope (SEM) observations of the fractured surface of UD-CFRP after the drop weight test suggested that the adhesion between carbon fiber and matrix resin was improved by the addition of sGF when the low impact energy was applied. The interlaminar shear strength of the modified UD-CFRP was also improved. The CAI strength of modified UD-CFRP was improved when the applied impact energy was relatively low. However, when the applied impact energy exceeds 7 J, the CAI strength of UD-CFRP was degraded by adding sGF. Therefore, when low impact loading was applied, the addition of sGF into UD-CFRP was effective to improve CAI strength.

Keywords: CAI test, CFRP, drop weight test, interlaminar shear test, split Hopkinson pressure bar method, sub-micron glass fiber.

1 INTRODUCTION

Carbon fiber reinforced plastics (CFRP) have been classified as one of the advanced composite materials because of their high strength despite their low density [1–3]. Therefore, it has been widely used in the fields where weight reduction is required, such as aircraft and space structures. It is also well known that CFRPs made by stacking the laminates are easily damaged and cause the delamination by out-of-plane impact [4–7]. The impact resistance of CFRPs must be improved to ensure the safety and reliability of structures. Yokozeki *et al.* [8] have suggested that the impact resistance of CFRPs by out-of-plane impact load was improved by using the toughened CFRP laminated with thin plies. Yamada *et al.* [9] have also proposed that the metal layers insertion in thin-ply composite laminates was improved Compressive after impact (CAI) strength by inhibiting the fiber break. A previous study done by Saravanakumar *et al.* [10] suggested that the modification of the resin matrix of CFRP by simply adding the sub-micron glass fiber (sGF) is effective to improve the Izod impact resistance of unidirectional (UD)-CFRP. However, the effect of sGF addition on the practical impact resistance such as the low-velocity impact resistance and CAI strength of CFRPs has not been investigated.

The purpose of this study is to investigate the effect of the sGF addition on the low-velocity impact resistance and CAI strength of UD-CFRP. Moreover, the effect of sGF addition on the

ISSN: 2046-0546 (paper format), ISSN: 2046-0554 (online), http://www.witpress.com/journals
DOI: 10.2495/CMEM-V10-N3-271-281

apparent interlaminar shear strength of UD-CFRP was also investigated. The two types of UD-CFRP in which matrix resin was modified or neat were prepared to conduct the low-velocity impact test. By using the dropping weight type test apparatus, the low-velocity impact load toward out-of-plane direction was applied to the UD-CFRP. The internal damage of UD-CFRP caused by impact was observed by phased array ultrasonic inspection machine. The apparent interlaminar shear strength of UD-CFRP was investigated by double-notch shear test under static and dynamic loading conditions.

2 MATERIALS AND METHODS

2.1 Materials

Thermoset epoxy resin (JER-828, Mitsubishi Chemical) and corresponding curing agent (Cure 113, Mitsubishi Chemical) were used as the matrix of the CFRP. The sGF (EFMW-1700, Nippon Muki) whose diameters and length are 0.69 and 71.6μm was used as the modifier of the resin matrix. Table 1 shows the material properties of matrix, reinforcement, and modifier, respectively.

2.2 Fabrication of modified resin

To fabricate the modified resin, the 0.30wt% of sGF was dispersed into the epoxy resin by mechanical stirring at 15,000 rpm for 30 min. After the dispersion process, the specified amount of curing agent was added to the modified resin. Before dispersing the sGF, the absorbed water in sGF was eliminated by heating. For comparison, the neat epoxy resin was also prepared.

2.3 Fabrication of UD-CFRP

The hand lay-up technique was employed to fabricate the UD-CFRP. The prepared resin was impregnated into a UD carbon fiber sheet by using a roller, then 10 sheets of impregnated UD carbon fiber sheets were stacked. The stacking sheets were preheated under 0.86 MPa at 80 deg-C for 1 h, then, hardened under 150 deg-C for 3 h by the heat pressing machine. The fiber volume fractions of the fabricated UD-CFRP were approximately 70vol%. The fabricated UD-CFRP was cut in parallel with the fibers using a diamond cutter to fabricate 60 × 100 × 3.5 mm³ of the strip-shaped specimen.

Table 1: Material properties of matrix and reinforcement.

	Material properties		
Materials	Tensile strength [MPa]	Young's modulus [GPa]	Fracture strain [%]
EPOXY RESIN	71.8	2.66	3.90
CARBON FIBER	4.12×10^3	235	1.80
SUB-MICRONGLASS FIBER	3.49×10^3	73.0	4.80

2.4 Low-velocity impact test

The energy absorption of the UD-CFRP under out-of-plane impact was investigated by low-velocity impact test with falling weight test apparatus, as shown in Fig. 1. The specimen was clamped by both longitudinal ends and a low-velocity impact load was applied by falling the impactor in which tip shape is 18 mm of a hemisphere. The displacement and load acting on the impactor were measured to calculate the energy absorption of UD-CFRP. The applied impact load to the specimen was calculated by the strain gauges adhered to the impactor. The displacement of the specimen was also measured by using the laser displacement sensor attached to the impactor. The applied impact energy for UD-CFRP was controlled to be 3, 5, 7, 10 and 20 J, respectively. In this study, the velocity of the impactor was approximately 4 m/s and at least five specimens were tested. The internal damage of UD-CFRP after the impact test was observed by phased array ultrasonic inspection apparatus (OmniScan SX, Olympus).

2.5 CAI test

The compressive strength of UD-CFRP after low-velocity impact test was measured to evaluate the CAI strength of UD-CFRP. To avoid the buckling of the specimen during a compressive test, the fixture [11] as shown in Fig. 2 was used. The 1.0 mm/min of compressive displacement was applied by a universal testing machine (Autograph, Shimadzu). At least five specimens were tested.

2.6 Double-notch shear test

The interlaminar shear strength of UD-CFRP was investigated using static and dynamic double-notch shear tests. The effect of fiber orientation and sGF addition on the apparent

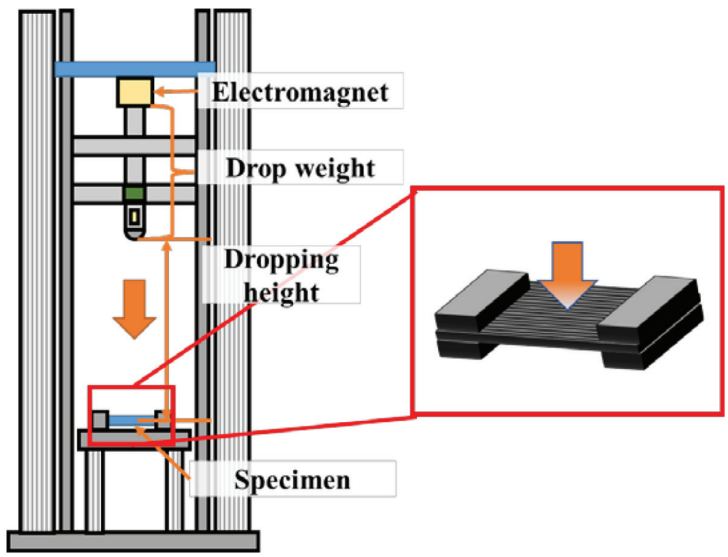

Figure 1: The schematic view of drop weight test apparatus.

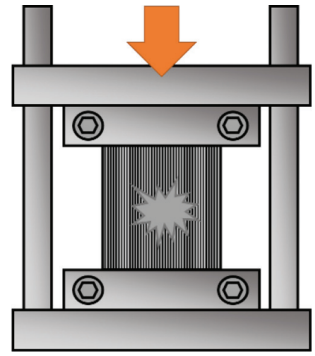

Figure 2: Specimen clamped method in CAI test.

interlaminar shear strength of UD-CFRP was investigated. In this study, two types of specimens in which laminate configurations are $[0_2/90_3]$s and $[0_5]$s are prepared. Figure 3 shows a schematic illustration of specimens for the double-notch shear test. Here, the machined notch is indicated by red lines. The notch of the specimen was machined by the diamond cutter. At least five specimens were tested. The apparent interlaminar shear strength τ_{ap} was calculated using eqn (1).

$$\tau_{ap} = \frac{P_{max}}{a \cdot b}. \tag{1}$$

Where P_{max}, a, and b denote the maximum load until failure, the distance between notches, and the width of the specimen, respectively.

2.6.1 Static interlaminar shear test

The static double-notch shear test was conducted following JIS-K7092 with the universal testing machine. The 1.0 mm/min of compressive displacement was applied to the end of the specimen.

2.6.2 Dynamic interlaminar shear test

The dynamic double-notch shear test was conducted with tensile-type split Hopkinson pressure bar apparatus, as shown in Fig. 4. The dynamic tensile load was applied by hitting the input bar (A5052, ∅20 × 1900) using an impactor (A5052, ∅55(φ30) × 200) driven by air pressure. By controlling the applied air pressure and opening time of the solenoid valve, the velocity of the impactor was controlled for controlling the applied strain rate. When the impactor hits the input bar, the tensile elastic stress wave propagates from the input bar to the output bar (A5052, ∅20 × 1500) through the specimen. The applied load P was measured by strain gauges adhered on both the input and output bars to evaluate the applied tensile force based on the one-dimensional elastic stress wave theory described in eqn (2).

$$\begin{aligned} \varepsilon(t) &= \frac{2C_b}{L_0}\int\left[\varepsilon_i(t) - \varepsilon_t(t)\right]dt \\ P(\mathrm{t}) &= A_b E \varepsilon_t(t) \end{aligned}. \tag{2}$$

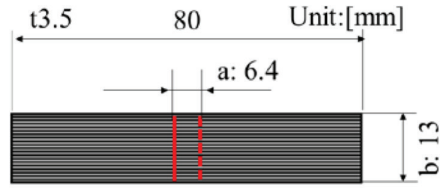

(a) Static strain rate condition.

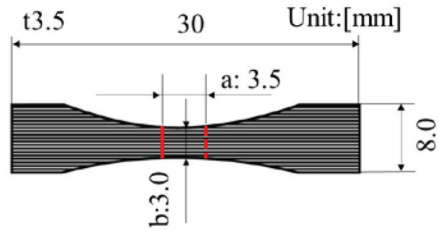

(b) Dynamic strain rate condition.

Figure 3: Specimen for interlaminar shear test.

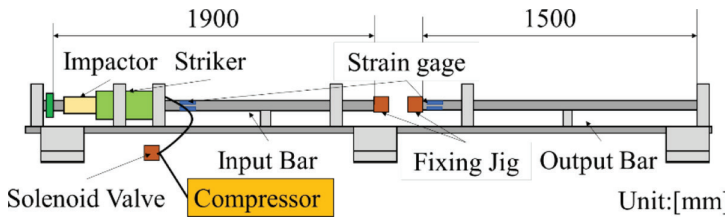

Figure 4: Split Hopkinson pressure bar apparatus.

Where $\varepsilon(t)$ is the strain on the specimen, C_b is the propagating velocity of longitudinal waves, E is the Young's modulus of input/output bar, A_b is the cross section area of input/output bar, $\varepsilon_i(t)$, $\varepsilon_t(t)$ are incident and transmitted strain, and L_0 is the length of the specimen, respectively.

3 RESULT AND DISCUSSION

3.1 Load–displacement curves of UD-CFRP in low-velocity impact tests

Figure 5 shows the typical load–displacement curves when the applied impact energy was 3 and 20 J, respectively. The peak load of UD-CFRP was slightly increased by adding sGF into its matrix when the applied impact energy was 3 and 5 J. In contrast, when the applied impact energy exceeds 7 J, there was no significant difference in peak load of UD-CFRP by the sub-micro glass fiber addition. These results suggested that when the applied impact energy was low, the addition of sGF is effective.

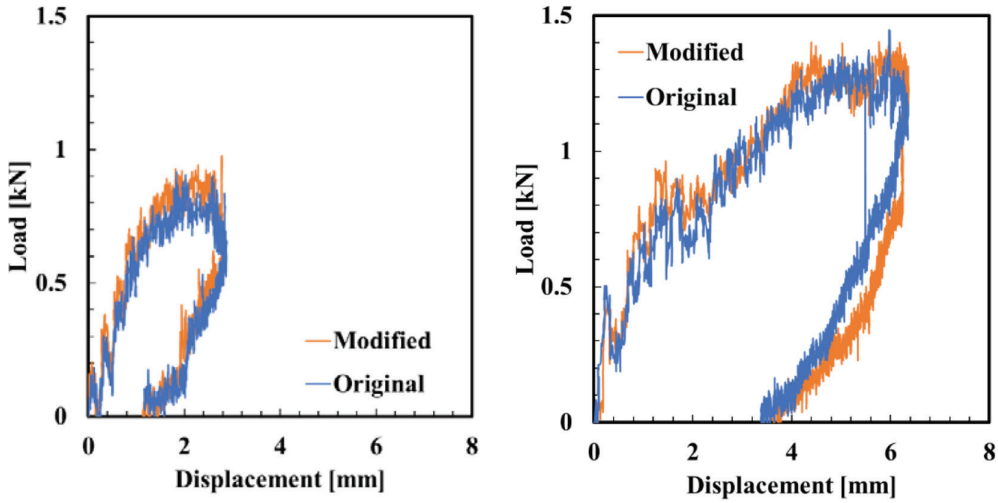

Figure 5: Load–displacement curves in drop weight test.

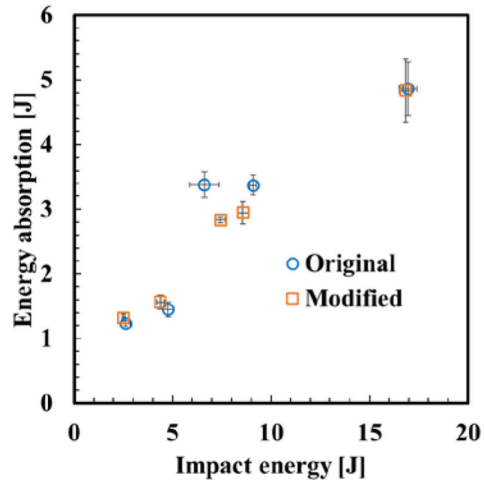

Figure 6: Energy absorption ratio of UD-CFRP in drop weight test.

3.2 Energy absorption of UD-CFRP in low-velocity impact test.

Figure 6 shows the energy absorption of UD-CFRP with respect to the applied impact energy. Here, the absorbed energy was calculated by the area enclosed by the load–displacement curve. Test results showed that the absorbed energy was increased with the increase of the applied impact energy. Moreover, when the applied impact energy was relatively low, the absorbed energy of UD-CFRP was improved by sGF addition. However, when the applied

impact energy exceeds 7 J, the improvement of the absorbed energy by sGF addition almost disappeared. These results suggested that the effect of sGF addition on the energy absorption ability of UD-CFRP was dependent on the applied impact energy.

3.3 Internal damages of UD-CFRP after low-velocity impact test

Figure 7 shows an ultrasonic observation result of internal damage of UD-CFRP after the impact test. Here, the white and blue colored region indicates the interlaminar delamination of UD-CFRP. Observation results showed that when the applied impact energy exceeds 7 J, the interlaminar delamination along the fiber direction of UD-CFRP reached the ends of the specimen. Moreover, when comparing the area of the delaminated region of UD-CFRP, the area of delamination seemed to be decreased by adding sGF.

Figure 8 also shows the SEM observation of UD-CFRP after the impact test. Observation results showed that the residue of the matrix on the fiber surface was confirmed when the applied impact energy was relatively low. However, when the applied impact energy exceeds 7 J, the residue of the matrix on the fiber surfaces seemed to be decreased. These

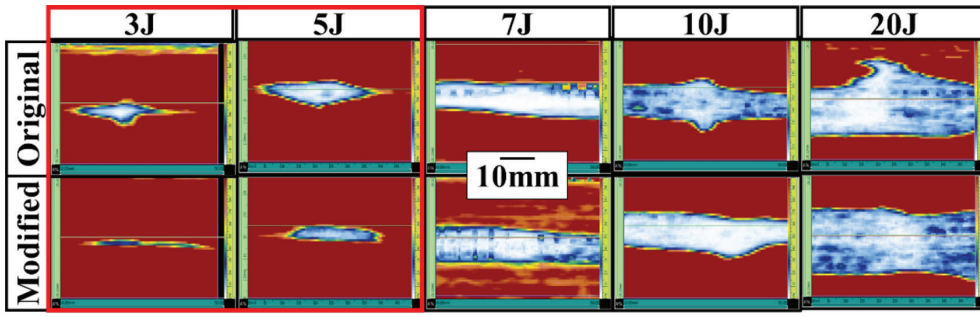

Figure 7: Projection image of internal damages after drop weight test.

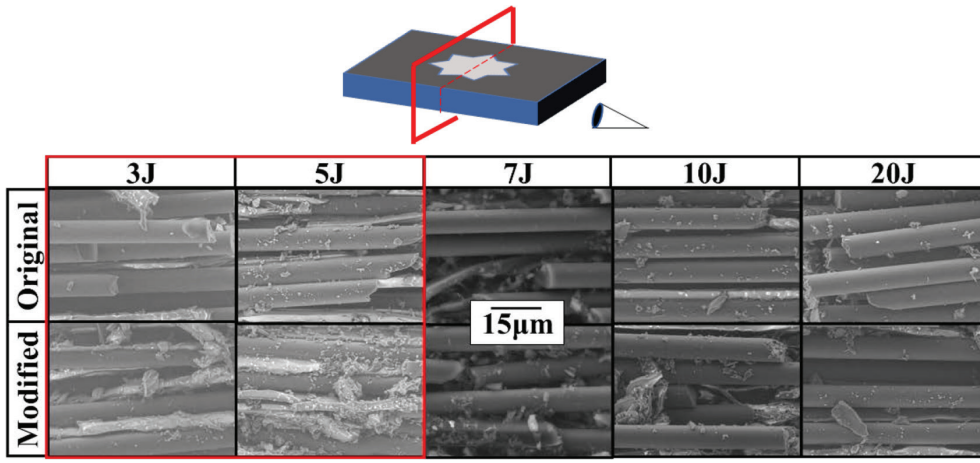

Figure 8: SEM observations of carbon fiber surface.

results indicated that adhesion between carbon fiber and epoxy matrix was improved by adding sGF.

3.4 CAI strength of UD-CFRP

Figure 9 shows the CAI strength of UD-CFRP with respect to the applied impact energy. The CAI strength of modified UD-CFRP was improved when the applied impact energy was relatively low. However, when the applied impact energy exceeds 7 J, the CAI strength of UD-CFRP was degraded by adding sGF. These results were explained as follows: when the applied impact energy was relatively low, the internal damage of UD-CFRP was suppressed by adding the sGF, therefore, the CAI strength of the UD-CFRP was improved.

3.5 Interlaminar shear strength of UD-CFRP in static and dynamic strain rate conditions.

Figures 10 and 11 show a typical stress strain diagram of the double-notch shear test under static and dynamic loading conditions. Test results showed that the almost same tendency of stress strain diagram until failure was confirmed even if the sGF was added into the matrix. However, the failure stress of the specimen seemed to be improved by adding the sGF into the matrix.

Figure 12 shows an apparent interlaminar shear strength along fiber and fiber orthogonal direction (0 deg and 90 deg) with respect to the applied strain rate. Test results showed that when the sGF was added into the matrix, the apparent interlaminar shear strength along the fiber direction (0 deg) was improved, while that along the fiber orthogonal direction was almost the same even after sGF addition. These results suggested that the effect of sGF addition on the interlaminar shear strength of UD-CFRP was dependent on the fiber direction.

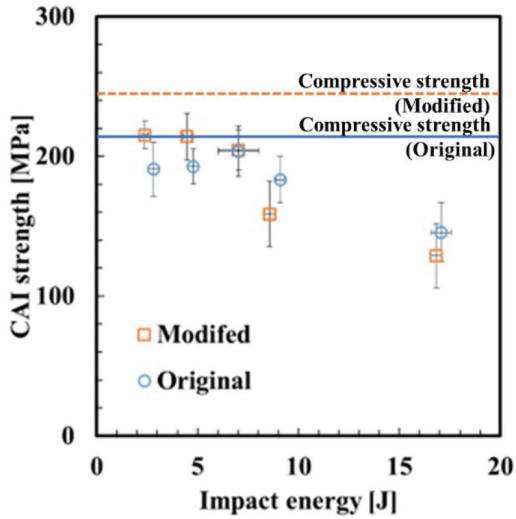

Figure 9: CAI strength of UD-CFRP with respect to impact energy.

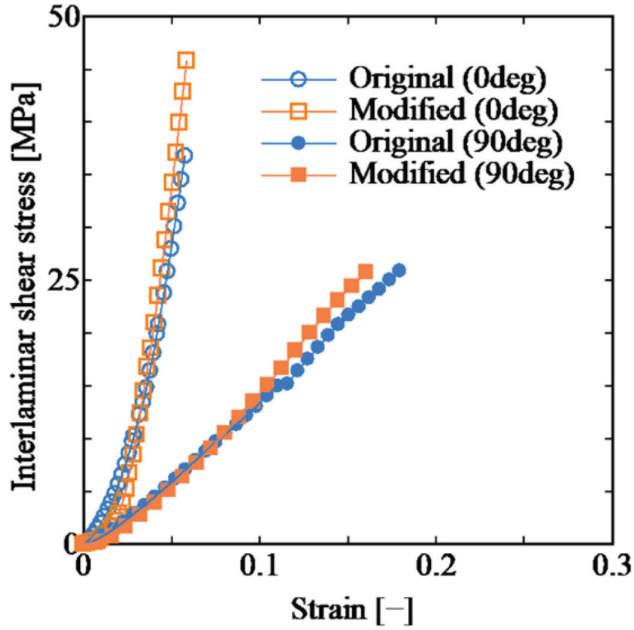

Figure 10: Typical stress–strain curves in static strain rate condition.

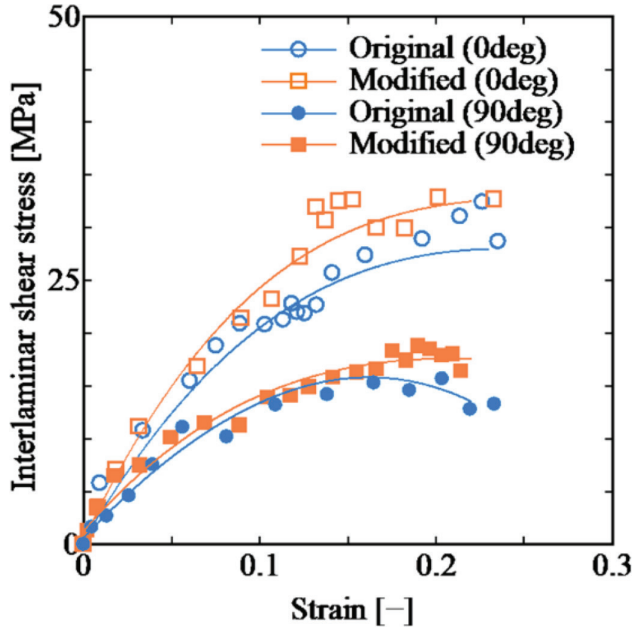

Figure 11: Typical stress–strain curves in dynamic strain rate condition.

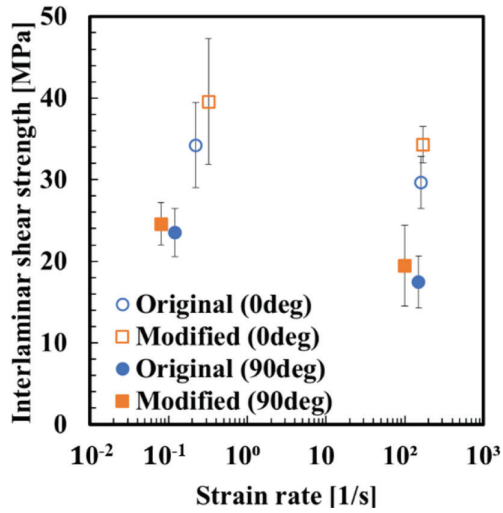

Figure 12: Interlaminar shear strength of UD-CFRP.

4 CONCLUSION

This study investigates the influence of the sGF addition on the energy absorption, CAI strength, and the interlaminar shear strength of UD-CFRP. The following conclusions were drawn:

1. The peak load of UD-CFRP was slightly increased by adding sGF into its matrix when the applied impact energy was 3 and 5 J. In contrast, when the applied impact energy exceeds 7 J, there was no significant difference in peak load of UD-CFRP by the sub-micro glass fiber addition.
2. The effect of sGF addition on the energy absorption ability of UD-CFRP was dependent on the applied impact energy.
3. When the applied impact energy exceeds 7 J, the area of delamination seemed to decrease by adding sGF.
4. When the applied impact energy was relatively low, the internal damage of UD-CFRP was suppressed by adding the sGF, therefore, the CAI strength of the UD-CFRP was improved.
5. The effect of sGF addition on the interlaminar shear strength of UD-CFRP was dependent on the fiber direction.

ACKNOWLEDGMENTS

The authors would like to thank Nippon Muki Co., Ltd. for their donation of sub-micron glass fiber. This work was partly supported by JSPS KAKENHI (Grant Number 21K03779).

REFERENCES

[1] Abena, A., Soo, S.L. & Essa, K., Modelling the orthogonal cutting of UD-CFRP composites. *Development of a novel cohesive zone model. Composite Structures*, **168**, pp. 65–83, 2017.

[2] Imamura, T. & Yamaguchi, Y., Progress of composite material for aircraft structure. *Journal of the Japan Society for Aeronautical and Space Sciences*, **43(495)**, pp. 213–223, 1995.
[3] Noziri, K., Properties required for the design of FRP for aircraft. *Materia Japan*, **39(11)**, pp. 897–900, 2000.
[4] Yang, B., Chen, Y., Lee, J., Fu, K. & Li, Y., In-plane compression response of woven CFRP composite after low-velocity impact: Modelling and experiment. *Thin-Walled Structures*, **158**, p. 107186, 2021.
[5] Iwahori, Y. & Ishikawa, T., Impact damage evaluation of interlaminar strength improved CFRP laminates. *The Japan Society of Mechanical Engineers*, **305(4)**, pp. 185–186, 2004.
[6] Ferrier, E., Rabinovitch, O. & Michel, L., Mechanical behavior of concrete-resin/adhesive-FRP structural assemblies under low and high temperatures. *Construction and Building Materials*, **127,** pp. 1017–1028, 2016.
[7] Liu, B., Gao, N., Cao, S., Ye, F., Liu, Y., Zhang, Y., Cheng, L. & Kikuchi, M., Interlaminar toughening of unidirectional CFRP with multilayers graphene and MWCNTs for mode II fracture. *Composite Structures*, **236**, p. 111888, 2020.
[8] Yokozeki, T., Aoki, Y. & Ogasawara, T., Damage behaviors and compressive strength of toughened CFRP laminates with thin piles subjected to transverse impact loadings. *Journal of the Japan Society for Aeronautical and Space Sciences, Japan*, **55(643)**, pp. 388–395, 2007.
[9] Yamada, K., Nishikawa, M., Kotter, B., Matsuda, N., Kawabe, K., Fiedler, B. & Hojo, M., Effect of ply-level hybridization and insertion of metal layers on impact damage modes and compression strength after impact of thin-ply composite laminates. *The Japan Society for Composite Materials*, **46(3)**, pp. 104–114, 2020.
[10] Saravanakumar, K., Arumugam, V., Souhith, R. & Santulli, C., Influence of milled glass fiber fillers on mode I & mode II interlaminar fracture toughness on epoxy resin for rabrication of glass/epoxy composites. *Fibres*, **8(6)**, p. 36, 2020.
[11] Kimpara, I., Kageyama, K., Suzuki, T. & Ohsawa, I., Simplified and unified approach to characterization of compressive residual strength of impact-damaged CFRP laminates. *Key Engineering Materials*, **141–143,** pp. 19–34, 1998.